Protection of the Retinal Ganglion Cells: Intravitreal Injection of Resveratrol in Mouse Model of Ocular Hypertension

Kejia Cao, Tomoka Ishida, Yuxin Fang, Kosei Shinohara, Xuejiao Li, Natsuko Nagaoka, Kyoko Ohno-Matsui, and Takeshi Yoshida

Department of Ophthalmology and Visual Science, Tokyo Medical and Dental University, Tokyo, Japan

Correspondence: Takeshi Yoshida, Department of Ophthalmology and Visual Science, Tokyo Medical and Dental University, 1-5-45 Yushima Bunkyo-ku, Tokyo 1138519, Japan; takec.oph@tmd.ac.jp.

Received: April 10, 2019
Accepted: January 9, 2020
Published: March 16, 2020

Citation: Cao K, Ishida T, Fang Y, et al. Protection of the retinal ganglion cells: intravitreal injection of resveratrol in mouse model of ocular hypertension. *Invest Ophthalmol Vis Sci.* 2020;61(3):13. https://doi.org/10.1167/iovs.61.3.13

Purpose. To investigate the efficacy of intravitreal administration of resveratrol (RSV) in a microbead-induced high intraocular pressure (IOP) murine model for glaucoma.

Methods. Experiments were performed using adult C57BL/6JJcl mice. Polystyrene microbeads were injected into the anterior chamber to induce IOP elevation. Retinal flat-mounts and sections were assessed by immunohistochemistry to detect the expression of reactive oxygen species and acetyl-p53 in retinal ganglion cells (RGCs), brain-derived neurotrophic factor (BDNF) in Müller glial cells (MGCs), and the receptor tropomyosin receptor kinase B (TrkB) in RGCs. Light cycler real-time PCR was also used for confirming gene expression of BDNF in primary cultured MGCs exposed to RSV.

Results. Microbeads induced high IOP followed by RGC death and axon loss. Administration of RSV rescued RGCs via decreased reactive oxygen species generation and acetyl-p53 expression in RGCs and upregulated BDNF in MGCs and TrkB expression in RGCs, which exhibited a strong cytoprotective action against cell death through multiple pathways under high IOP.

Conclusions. Our data suggest that administration of RSV may delay the progress of visual dysfunction during glaucoma and may therefore have therapeutic potential.

Keywords: resveratrol, glaucoma, retinal ganglion cell, high intraocular pressure, reactive oxygen species, p53, Müller glial cells

Glaucoma is the leading cause of irreversible blindness worldwide.[1,2] The disease is characterized by progressive degeneration of retinal ganglion cells (RGCs) projecting into the brain.[3,4] A major risk factor for this disease is elevated intraocular pressure (IOP).[5] Currently, the only clinically effective glaucoma treatment is oriented toward lowering IOP.[6,7] Neuroprotective interventions against glaucoma, which may have therapeutic potential, have not been thoroughly explored.[8,9]

Oxidative stress (OS) generates reactive oxygen species (ROS).[10–12] Recent studies using experimental glaucoma models and clinical samples have demonstrated that OS is present in ocular tissue, indicating its potential role in the pathogenesis of glaucoma.[13,14] The mechanisms by which OS may induce RGC loss are not fully understood but may include direct neurotoxic effects from ROS or indirect damage from OS-induced dysfunction of glial cells.[15] Tumor suppressor p53 is a redox active transcription factor that organizes and directs cellular responses against a variety of stresses; it regulates the cell cycle, in particular by eliminating cells with lethal insults via induction of apoptosis.[16] Guo et al.[17] demonstrated that an increase in retinal p53 mRNA levels is positively correlated with optic nerve injury due to elevated IOP. Experimentally, it has been shown that inhibitors and enhancers of p53 modulate RGCs survival.[18,19] Furthermore, clinical studies have revealed associations between specific p53 haplotypes and polymorphisms with the progression of primary open-angle glaucoma in human,[20–22] emphasizing the potential importance of p53 in RGCs death. Recent studies have revealed that cell-generated ROS and p53 are implicated in mediating apoptosis.[23,24]

Resveratrol (RSV), a natural polyphenolic compound, is known as an activator of Sirtuin 1 (Sirt1), a class III histone deacetylase dependent on nicotinamide adenine dinucleotide. Sirt1 regulates cell senescence, DNA damage repair, and apoptosis and controls longevity in response to caloric restriction in numerous mammals.[25–27] It is therefore thought to have several health-enhancing properties. Indeed, many clinical studies have highlighted the beneficial effects of RSV in human diseases.[28–32] RSV has also been suggested as a protective agent in preventing and treating organ injury due to its antioxidative properties.[33–36] Pirhan et al.[37] showed that intraperitoneal administration of RSV delays RGC loss in an experimental glaucoma model; however, the underlying molecular mechanisms behind this phenomenon are unknown. Notable progress has been made in identifying the critical role of retinal Müller glial cells (MGCs) in maintaining retinal homeostasis through the expression of various

neuroprotective signaling molecules[38–40] protecting the retina from many stresses, including OS.[41] Among various neuroprotective signaling molecules that MGCs express, brain-derived neurotrophic factor (BDNF) is known to be a potent neurotrophic molecule. Harada et al.[42,43] previously reported that brimonidine, a selective α_2-adrenergic receptor agonist, stimulates the expression of BDNF in MGCs and promotes RGC survival. In the present study, we used a murine model of high IOP to characterize and study the implications of retinal OS and p53 expression on IOP-induced RGC cell death in response to intravitreal RSV administration. Using this model, we also studied the changes in the expression of BDNF in MGCs in response to intravitreal administration of RSV. We revealed that intravitreal injection of RSV upregulates Sirt1 expression in RGCs and rescues RGCs from high IOP-induced RGCs cell death by multiple pathways, including reduced ROS generation and acetyl-p53 expression in RGCs. We also revealed that intravitreal injection of RSV activates MGCs and upregulates a potent neurotrophic factor, BDNF, to rescue RGCs from cell death induced by high IOP.

Methods

Animal

All animal study protocols were approved by the Animal Care and Use Committee of Tokyo Medical and Dental University (Permit No. A2017-328A). All procedures were carried out in accordance with the Association for Research in Vision and Ophthalmology Statement for the Use of Animals in Ophthalmic and Vision Research. A total of 75 adult male C57BL/6JJcl mice (CLEA Japan, Tokyo, Japan) were divided into five groups: control, microbead injection, microbead injection with 3-µM RSV, microbead injection with 30-µM RSV, and 30-µM RSV injection ($n = 15$ in each group). All mice were anesthetized using 40 mg/kg pentobarbital (Kyouritu Seiyaku Corporation, Tokyo, Japan), and their pupils were dilated with 0.5% phenylephrine hydrochloride and 0.5% tropicamide (Santen Pharmaceutical Co., Ltd., Tokyo, Japan).

Induction and Measurement of IOP Model

High IOP was induced using microbeads as described in previous studies.[3,44,45] Microbead-injected mice groups received 3 µl of 10-µm-diameter polystyrene microbeads (Polysciences, Inc., Warrington, PA, USA) at a final concentration of 4.55×10^6 microbeads per milliliter, via a 35-gauge needle, into the anterior chamber of the right eye. Mice in the control group received an injection of the same volume, but of Gibco PBS (Thermo Fisher Scientific, Waltham, MA, USA). IOP was measured every second day using a Tono-Pen AVIA tonometer (Reichert Technologies, Depew, NY, USA). Prior to measurement, mice were anesthetized using pentobarbital. The mean of six readings in each eye was utilized to calculate IOP.

Intravitreal Injection of RSV

Mice were administered 1 µl of 3-µM or 30-µM RSV (Tokyo Chemical Industry Co., Ltd., Tokyo, Japan) dissolved in PBS by injection into the right eye with a 35-gauge needle in the vitreous body on the same day after the microbead injection. As control, 1 µl of PBS was injected into the left eye. To prevent infection, ofloxacin ointment (Santen Pharmaceutical Co., Osaka, Japan) was applied.

Flat-Mount Retina Immunohistochemistry

To make the retinal flat-mounts, mice eyes were enucleated and fixed in 4% paraformaldehyde overnight at 4°C. The cornea and lens were removed, and the entire retina was carefully dissected from the eyecup. Radial cuts (average of four) were made from the edge of the eyecup to the equator and then washed with PBS containing 0.5% Triton X-100 (Bio-Rad, California, USA), as described previously.[46–48] For Brn-3a-positive RGC counts on flat-mounts, the retinas were stained overnight at 4°C with mouse anti-Brn-3a monoclonal antibody (1:100; Santa Cruz Biotechnology, Dallas, TX, USA). The retinas were then incubated with anti-mouse IgG for 2 hours at room temperature (RT). For quantification of Brn-3a-positive RGCs, each retinal quadrant was further subdivided into regions of acquisition defined as the peripheral retina (the retinal portion 2.5 mm from the optic nerve head) or the central retina (the retinal portion in the nearby area, 1 mm from the optic nerve head). We took eight images (290 µm × 290 µm) each of the peripheral retina and central retina (total four images per quadrant, 16 images per eye) under masked conditions using a confocal microscope (SP8; Leica Camera AG, Wetzlar, Germany). In this way, labeled cells were identified, counted, and pooled together, as described previously.[49–52] All data were quantified using ImageJ software v1.51 (National Institutes of Health, Bethesda, MD, USA) as previously described,[53–55] which automatically calculated the number of Brn-3a-positive cells per image and the density of Brn-3a cells/mm^2 of retina in the five groups.

Retinal Section Preparation

All mice were euthanized at 21 days after microbead and/or RSV injection, as previously reported.[45,56–58] To prepare frozen sections, eyes were enucleated and embedded in optimal cutting temperature (OCT) compound (Sakura Finetek Japan, Tokyo, Japan) frozen in liquid nitrogen. The frozen blocks were cut into 10-µm sagittal retinal sections with a full length of retina through the ora serrata and optic nerve, using a Leica CM3050 S Cryostat, as previously described.[59,60] To make paraffin sections, the eyes were enucleated and dipped in Carnoy's solution (absolute ethanol:chloroform:glacial acetic acid, 6:3:1) for 3 hours at 4°C and then dehydrated and embedded in paraffin for processing to 4-µm paraffin sections.[59,60] We selected the sections with a full length of retina through the ora serrata and optic nerve and observed regions at a distance of 100 to 200 µm from the center of the optic nerve in all radial retinal sections, as described previously.[61] Four regions from six sections per retina were prepared and used for statistical analysis.

Dihydroethidium Staining for ROS

To detect the generation of ROS in retina, fresh frozen sections incubated with 0.1 µmol/L dihydroethidium (Invitrogen Molecular Probes, Thermo Fisher Scientific) in a light-protected, humidified chamber at 37°C for 30 minutes, as described previously.[62] Nuclei were stained with 4′,6-diamidino-2-phenylindole (DAPI; Vector Laboratories, Inc., Burlingame, CA, USA).

Investigative Ophthalmology & Visual Science

TUNEL Assay

For the detection of apoptotic RGCs, terminal deoxynucleotidyl transferase dUTP nick end labeling (TUNEL) staining was performed using an in situ cell death detection kit (Roche, Mannheim, Germany), as described previously.[63] Before staining, the paraffin sections were dewaxed, rehydrated, and incubated with a proteinase K working solution (Wako Pure Chemical Industries, Ltd., Osaka Japan) per the manufacturer's protocol. Fluorescein isothiocyanate immunofluorescence was then used, and the nuclei were co-stained with DAPI.

Immunohistochemical Analysis

Paraffin sections were dewaxed, rehydrated, and heated in a plastic jar containing 200 ml of 0.1-M citrate buffer with a pH of 6.0 under microwave irradiation for 10 minutes at 350 W. Sections were cooled to RT and washed three times with PBS. The sections were blocked in 10% normal goat serum (Vector Laboratories) in PBS and incubated with mouse anti-Brn-3a monoclonal antibody (1:100; Santa Cruz Biotechnology), rabbit anti-Sirt1 primary antibody (1:200; Cell Signaling Technology, Inc., Boston, MA, USA), mouse anti-neurofilament H (clone SMI32) primary antibody (1:1000; Covance, Princeton, NJ, USA), rabbit anti-glia fibrillary acidic protein (GFAP) antibody (1:1; Dako, Carpentaria, CA, USA), mouse anti-BDNF antibody (1:100; Abcam, Cambridge, MA, USA), anti-glutamine synthetase antibody (1:5000; Abcam), and rabbit anti-tropomyosin receptor kinase B (TrkB) antibody (1:250; Abcam) overnight at 4°C. Anti-acetyl-p53 (1:200; Flarebio Biotech LLC, College Park, MD, USA) was stained using a fluorescein-based M.O.M. Immunodetection Kit (Vector Laboratories). The sections were washed with PBS three times before they were incubated with an appropriate fluorophore-conjugated secondary antibody for 1 hour. All sections were mounted with DAPI and imaged with an SP8 confocal microscope, and all data were quantified using ImageJ software, as described earlier.[64,65]

Cell Culture

MGCs were isolated from murine pup eyes (postnatal days 4–5) and cultured as described previously.[42] In brief, MGCs were seeded onto 35-mm dishes (Ibidi GmbH, Martinsried, Germany) and cultured in Dulbecco's Modified Eagle's Medium (DMEM; Sigma-Aldrich, St. Louis, MO, USA) containing 100 U/ml penicillin, 100 µg/ml streptomycin (Wako Pure Chemical Industries), and 10% fetal bovine serum (FBS; Biowest, Nuaille, France). Cultures were maintained at 37°C in a humidified 95% air/5% CO_2 atmosphere.

Cell Viability Assay

The viability of MGCs was determined using a Cell Counting Kit-8 (CCK-8) assay (Dojindo Laboratories, Kumamoto, Japan), as in previous studies.[66,67] The isolated and cultured mouse MGCs were plated in 96-well plates (5×10^3 cells per well) and incubated for 24 hours. RSV was diluted in DMEM with 0.2% dimethyl sulfoxide (Sigma-Aldrich), and the vehicle was used as control. MGCs were then treated with different concentrations of RSV (3, 30, 70, and 140 µM) in culture medium for 6 hours. Then, 10 µl of CCK-8 solution was added to each well in the dark followed by incubation for 2 hours at 37°C. Measurements of optical density were obtained at a wavelength of 450 nm using a microplate reader (Bio-Rad Laboratories, Inc., Hercules, CA, USA). Each experiment was performed in triplicate.

Light Cycler Real-Time PCR

One-hundred percent confluent MGCs were incubated with 3-, 30-, 70-, or 140-µM RSV for 6 hours following the previous study protocol,[40] as well as cell viability assay. Total RNA was extracted from cultured MGCs using an illustra RNAspin Mini RNA Isolation Kit (GE Healthcare, Amersham, UK). cDNA was synthesized from 1 µg total RNA using the ReverTra Ace (Toyobo Co., Osaka, Japan) according to the manufacturer's instructions. Semiquantitative PCR was performed using KAPA SYBR FAST qPCR Master Mix (Kapa Biosystems, Inc., Boston, MA, USA), and a Roche LightCycler 480 Instrument II system was used to detect the gene expression of BDNF. We used a β-actin primer as a normalization factor that was commercially purchased (Qiagen, Hilden, Germany). The amplification schedule was as follows: initial denaturation at 95°C, followed by 45 cycles of 95°C for 30 seconds, 55°C (BDNF and β-actin) for 1 minute, and 72°C for 30 seconds. The following primer sequences were used: BDNF forward, 5′-ctgagcgtgtgtgacagtatt-3′, and reverse, 5′-ctttggataccgggactttctc-3′ (GenBank accession number: NM_001316310.1). The relative change in mRNA expression was calculated using $\Delta\Delta$CT values, and each experiment was performed in triplicate. Levels were normalized to those of β-actin and reported as fold change compared with the controls.

Western Blot Analysis

The protein expression of Sirt1, acetyl-p53, BDNF, and TrkB in the whole retina were analyzed by western blot. After mice eyeballs were enucleated, the retina and sclera were isolated. Protein lysates were extracted using RIPA Lysis Buffer (Thermo Fisher Scientific) supplemented with protease inhibitor (Sigma-Aldrich), according to the manufacturers' protocol. Briefly, all lysates were quantified, and equal volumes were loaded on NuPAGE 4–12% Bis-Tris gel (Invitrogen) before being transferred to polyvinylidene difluoride membranes (Invitrogen). Membranes were blocked with 3% skim milk and incubated with anti-Sirt1 primary antibodies (1:1000; Cell Signaling Technology), anti-acetyl-p53 (1:400; Abcam), rabbit anti-BDNF antibody (1:500; GeneTex, San Antonio, TX, USA), and rabbit anti-TrkB antibody (1:1000; Abcam) overnight at 4°C. Bound proteins were detected using peroxidase-conjugated ECL anti-mouse IgG and anti-rabbit (GE Healthcare UK). Proteins were visualized using a chemiluminescence substrate (Bio-Rad Laboratories) and imaging system (DNR Bio Imaging Systems, Neve Yamin, Israel). Glyceraldehyde-3-phosphate dehydrogenase was used as a loading control. The expression ratios of protein bands were quantified using ImageJ, as previous described.[68]

Statistics

Quantitative data were expressed as mean ± SD. Data analysis was performed by SPSS Statistics 24.0 (IBM, Armonk, NY, USA) using Student's *t*-test, one-way ANOVA, and Tukey post hoc test to compare two or more groups. Statistical differences were considered significant for $P < 0.05$.

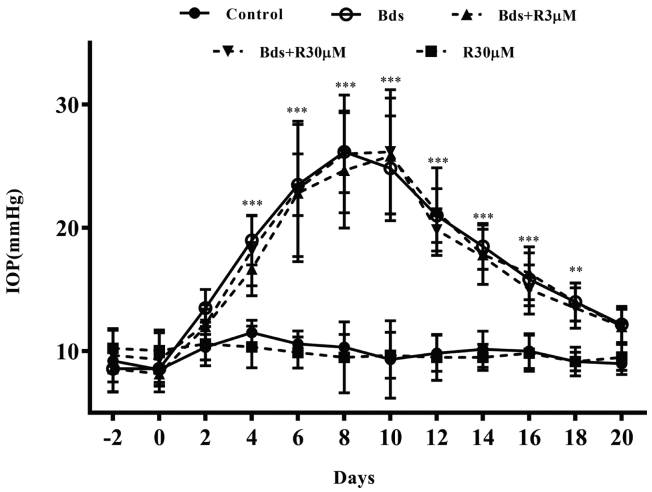

Figure 1. Measurement of IOP in a microbead-injection-induced experimental glaucoma model. Average IOP measures of all experimental groups ($n = 9$). IOP values are expressed as the mean ± SD for each time point; $^{*}P < 0.05$, $^{**}P < 0.01$, $^{***}P < 0.001$ compared with the control group (Student's *t*-test). Control, PBS injection group; Bds, microbead injection group; Bds+R3μM, microbead injection with 3-μM RSV injection group; Bds+R30μM, microbead injection with 30-μM RSV injection group; R30μM, 30-μM RSV injection alone group.

Results

Change in Intraocular Pressure After Microbead Injection

The IOP of the mice was measured every 2 days following the microbead injections. Mice in the control group that received an injection of PBS exhibited a steady IOP level (9.8 ± 1.5 mm Hg) throughout the experimental period. Compared with the control group, an elevation in IOP was induced at 4 days after injection in the microbead and microbead + RSV groups. There were significant differences in the microbead group and the microbead + RSV groups compared with the control group on days 4 to 18 ($P < 0.001$) (Fig. 1). The elevated IOP levels reached a peak of 26.2 ± 4.3 mm Hg on the 8th day after injection in the microbead group, 25.8 ± 4.7 mm Hg on the 10th day after injection in the microbead + 3-μM RSV group, and 26.2 ± 5.0 mm Hg on the 10th day after injection in the microbead + 30-μM RSV group. The mean IOPs were 17.1 ± 6.2 mm Hg in the microbead group, 17.4 ± 6.9 mm Hg in the microbead + 3-μM RSV group, and 16.9 ± 6.4 mm Hg in the microbead + 30-μM RSV group throughout the experimental period. These IOPs were, respectively, 1.7-, 1.8-, and 1.7-fold higher than the IOP of the control group. The group that received 30-μM RSV injections alone showed no significant differences compared with the controls ($P = 0.867$) (Fig. 1) at all time points throughout the experimental period, demonstrating that RSV does not affect IOP.

Administration of RSV Increased Sirt1 Expression Under Microbead-Induced High IOP

As shown in Figure 2, to quantify the expression of Sirt1 in RGCs, we used double immunofluorescence staining for Sirt1 and Brn-3a in the retina sections. Quantitative analysis showed that Sirt1-positive fluorescence area was significantly decreased in the microbead-injected group compared with the controls (3.9 ± 1.5% vs. 11.0 ± 3.3%; $P < 0.01$) (Figs. 2Aa–2Ah, 2B). Treatment with 3-μM RSV did not significantly alter Sirt1 expression in RGCs compared with microbead injection alone (5.8 ± 3.6%; $P = 0.801$) (Figs. 2Ai–2Al, 2B). However, administration of 30-μM RSV recovered the expression of Sirt1 in the RGCs to approximately control levels (8.8 ± 2.3%; $P = 0.726$) (Figs. 2Am–2Ap, 2B). The group receiving injections of only 30-μM RSV had no significant difference compared with the control group (11.2 ± 4.2%; $P > 0.999$) (Figs. 2Aq–2At, 2B). Sirt1 protein levels of whole retina in western blot analysis showed similar patterns in all groups (Supplementary Fig. S1).

Administration of RSV Affects RGCs Responses to Microbead-Induced High IOP

RGCs were quantified via staining of retina flat mounts with Brn-3a (Fig. 3), a specific marker for alive RGCs,[60,69,70] and via staining of cross-sections with SMI-32 (Fig. 4), an antibody directed against neurofilament H in the axons of RGCs. Figure 3A shows a low-magnification image of a flat-mounted retina divided into four quadrants centered on the optic nerve head, which marked all analyzed regions per retina. The mean numbers of Brn-3a-labeled RGCs in the control group were 2409.8 ± 76.4 in the central retina (Figs. 3Ba, 3C) and 2025.4 ± 65.5 in the peripheral retina (Figs. 3Bf, 3C). Brn-3a-labeled RGCs were significantly reduced in number in both the central retina (mean cell density 1787.6 ± 184.8; $P < 0.05$) (Figs. 3Bb, 3C) and peripheral retina (mean cell density 1208.9 ± 364.6; $P < 0.05$) (Figs. 3Bg, 3C) of the microbead group compared with the control group (Figs. 3Ba, 3Bf).

Treatment with 3-μM RSV did not result in a significant difference in the number of Brn-3a-labeled RGCs in either the central retina (mean cell density 1807.4 ± 220.2; $P > 0.999$) (Figs. 3Bc, 3C) or peripheral retina (mean cell density 1470.5 ± 153.4; $P = 0.478$) (Figs. 3Bh, 3C) compared with the group receiving only microbead injections. However, Brn-3a-labeled RGCs significantly increased in number in both the central retina (mean cell density 2302.8 ± 327.8; $P < 0.05$) (Figs. 3Bd, 3C) and the peripheral retina (mean cell density 1759.8 ± 132.4; $P < 0.05$) (Figs. 3Bi, 3C) of the microbead + 30-μM RSV group compared with the group receiving only microbead injections. The number of Brn-3a-labeled RGCs recovered to almost the level of the control group. The group receiving 30-μM RSV injections alone had no significant difference compared with the control group in either the central retina (mean cell density 2227.5 ± 127.1; $P = 0.811$) (Figs. 3Be, 3C) or peripheral retina (mean cell density 1969.9 ± 24.8; $P = 0.996$) (Figs. 3Bj, 3C). Additionally, a decrease in the SMI-32-positive fluorescence area was observed in the ganglion cell layer (GCL) of microbead-injected eyes (2.9 ± 1.0%; Figs. 4Ad–4Af, 4B) compared with controls (13.6 ± 4.0%; Figs. 4Aa–4Ac, 4B) ($P < 0.001$). The 3-μM RSV injection produced no significant change in SMI-32-positive fluorescence area compared to microbead injection alone (3.7 ± 2.0%; $P = 0.99$) (Figs. 4Ag–4Ai, 4B). However, 30-μM RSV significantly increased SMI-32-positive fluorescence compared to the microbead injection alone (12.1 ± 2.9%; $P < 0.001$) (Figs. 4Aj–4Al, 4B). There was no significant difference between the 30-μM RSV injection group

Investigative Ophthalmology & Visual Science

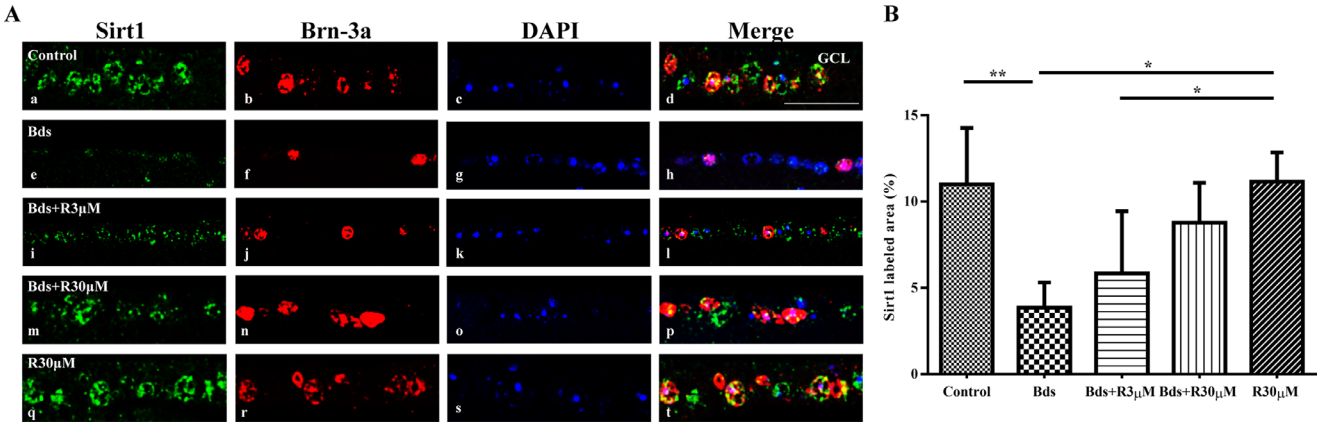

Figure 2. Quantitative analysis of Sirt1 expression in RGCs among the five groups. (**A**) Representative photographs of double immunofluorescence staining for Sirt1 (green) and Brn-3a (red) expression in the GCL in all groups at day 21 post-injection. Nuclei were labeled with DAPI staining (blue). (**B**) The percentages of Sirt1-labeled fluorescence areas in the GCL were measured. *Scale bar*: 50 µm. The data are presented as the mean ± SD ($n = 6$). Asterisks indicate statistical differences ($^{*}P < 0.05$, $^{**}P < 0.01$, $^{***}P < 0.001$) as determined by one-way ANOVA with Tukey as post hoc test. Control, PBS injection group; Bds, microbead injection group; Bds+R3µM, microbead injection with 3-µM RSV injection group; Bds+R30µM, microbead injection with 30-µM RSV injection group; R30µM, 30-µM RSV injection alone group.

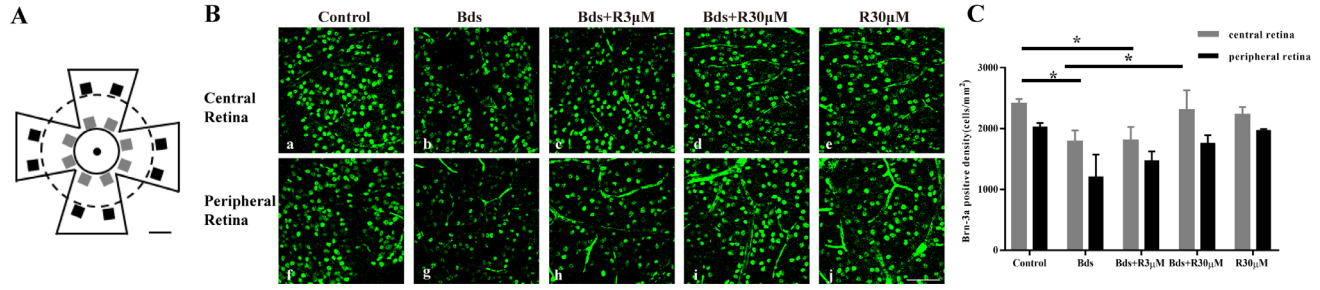

Figure 3. Quantitative analysis of Brn-3a-labeled RGCs among the five groups. (**A**) Schematic diagram of a flat-mounted retina showing all analyzed regions per retina. Different retinal fields in the central retina (gray box at distance 1 mm from the optic nerve head) and peripheral retina (black box at distance 2.5 mm from the optic nerve head) were acquired along the four quadrants centered on the optica nerve head. *Scale bar*: 1 mm. (**B**) Representative photographs from central retina (Ba–Be) and peripheral retina (Bf–Bj) showing RGCs labeled with Brn-3a (green) RGCs at day 21 post-injection. *Scale bar*: 75 µm. (**C**) Mean cell density of RGCs expressing Brn-3a (cells/mm^2) in the central and peripheral retina of five groups. The data are presented as the mean ± SD ($n = 3$). Asterisks indicate statistical differences ($^{*}P < 0.05$, $^{**}P < 0.01$, $^{***}P < 0.001$) as determined by one-way ANOVA with Tukey as post hoc test. Control, PBS injection group; Bds, microbead injection group; Bds+R3µM, microbead injection with 3-µM RSV injection group; Bds+R30µM, microbead injection with 30-µM RSV injection group; R30µM, 30-µM RSV injection alone group.

(13.3 ± 4.5%) (Figs. 4Am–4Ao) and the control group ($P > 0.999$).

RSV-Inhibited ROS Generation Resulted in Decreased RGC Death in a Murine High-IOP Model

Dihydroethidium staining showed that ROS generation contributes to RGC death due to high IOP (Fig. 5). TUNEL staining was used to detect subsequent cell death (Fig. 6). As shown in Figure 5, the percentages of ROS-generated area in the control group was 1.0 ± 0.5% (Figs. 5Aa–5Ac, 5B); however, microbead injection alone significantly increased the area of ROS generation to 13.6 ± 3.5% ($P < 0.001$) (Figs. 5Ad–5Af, 5B). Although the 3-µM RSV injections did not significantly decrease ROS generation in RGCs compared with the microbead-injected group (11.9 ± 4.6%; $P = 0.777$) (Figs. 5Ag–5Ai, 5B), the 30-µM RSV injections significantly decreased ROS accumulation in RGCs compared to the microbead-injected group (1.7 ± 1.1%; $P < 0.001$) (Figs. 5Aj–5Al, 5B). Notably, 30-µM RSV administration attenuated ROS accumulation, returning it to control levels ($P = 0.992$). There was no significant difference between the control group and the group receiving 30-µM RSV injections alone (1.0 ± 0.8%; $P > 0.999$) (Figs. 5Am–5Ao, 5B).

As shown in Figure 6, TUNEL-positive RGCs were significantly increased in the group receiving microbead injections alone (65.5 ± 16.4%; $P < 0.001$) (Figs. 6Ad–6Af, 6B). The 30-µM RSV treatment after microbead injection markedly decreased TUNEL-positive RGCs compared with microbeads alone (19.1 ± 15.0%; $P < 0.001$) (Figs. 6Aj–6Al, 6B). These findings indicated that 30-µM RSV led to a drastic increase in cell survival under high IOP, whereas 3-µM RSV did not significantly decrease the number of TUNEL-positive RGCs

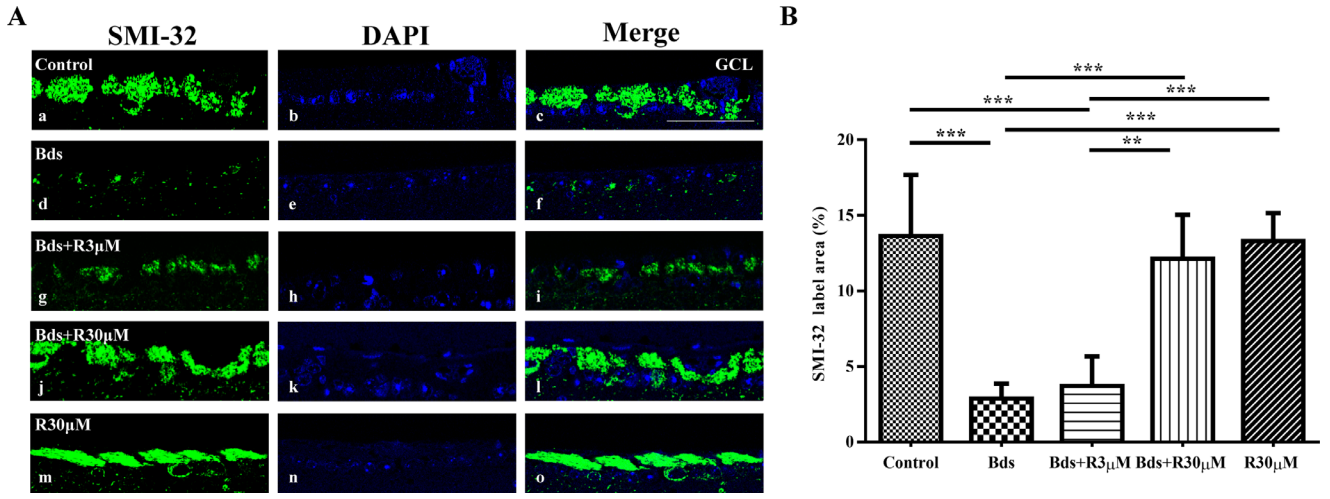

Figure 4. Quantitative analysis of SMI-32 expression among the five groups. (**A**) Representative photographs of RGC axons labeled with SMI-32 (green) expressed in all groups at day 21 post-injection. Nuclei were labeled with DAPI staining (blue). (**B**) The percentages of SMI-32-labeled fluorescence areas in the GCL were measured. *Scale bar*: 50 µm. The data are presented as the mean ± SD ($n = 6$). Asterisks indicate statistical differences ($^{*}P < 0.05$, $^{**}P < 0.01$, $^{***}P < 0.001$) as determined by one-way ANOVA with Tukey as post hoc test. Control, PBS injection group; Bds, microbead injection group; Bds+R3µM, microbead injection with 3-µM RSV injection group; Bds+R30µM, microbead injection with 30-µM RSV injection group; R30µM, 30-µM RSV injection alone group.

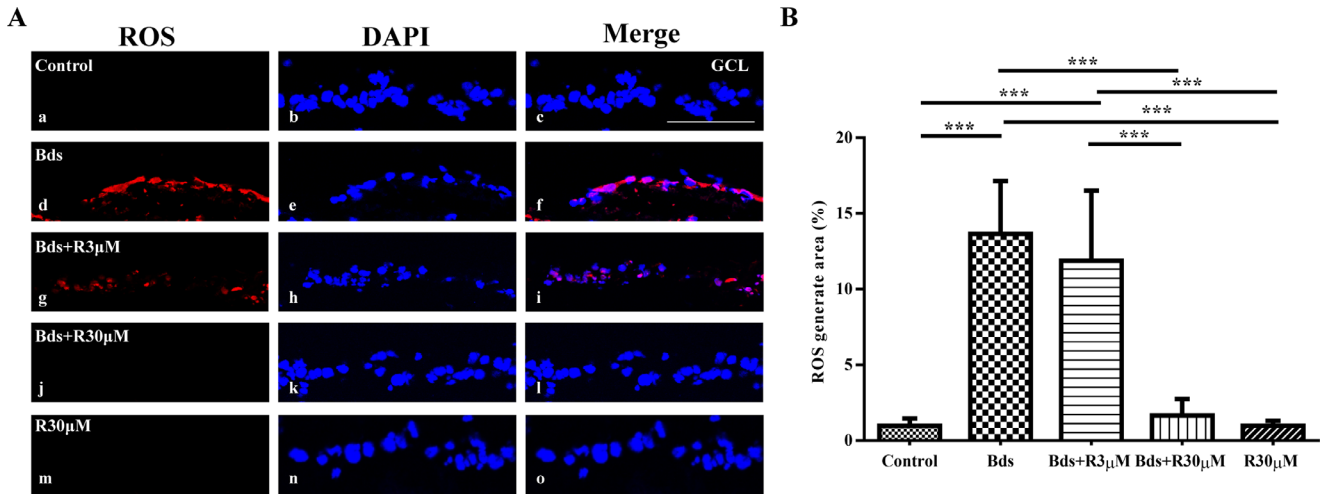

Figure 5. Quantitative analysis of ROS generation among the five groups. (**A**) Representative photographs of ROS expression in all groups at day 21 post-injection. Nuclei were labeled with DAPI staining (blue). (**B**) The percentages of ROS-generated fluorescence areas in the GCL were measured. *Scale bar*: 50 µm. The data are presented as the mean ± SD ($n = 6$). Asterisks indicate statistical differences ($^{*}P < 0.05$, $^{**}P < 0.01$, $^{***}P < 0.001$) as determined by one-way ANOVA with Tukey as post hoc test. Control, PBS injection group; Bds, microbead injection group; Bds+R3µM, microbead injection with 3-µM RSV injection group; Bds+R30µM, microbead injection with 30-µM RSV injection group; R30µM, 30-µM RSV injection alone group.

(58.2 ± 8.0%; $P = 0.801$) (Figs. 6Ag–6Ai, 6B). In addition, there is no significant difference between the control group (4.8 ± 5.4%; Figs. 6Aa–6Ac, 6B) and the group receiving the 30-µM RSV injection alone (6.7 ± 2.0%; Figs. 6Am–6Ao, 6B) ($P = 0.999$).

RSV Downregulated the Expression of High IOP-Induced Acetyl-p53 in RGCs

As shown in Figure 7, the expression of the acetyl-p53 in the GCL was studied. Quantitative analysis confirmed that a significantly higher acetyl-p53-positive fluorescence area was observed in the microbead injection group compared with the control group (6.7 ± 2.3% vs. 1.0 ± 1.4%; $P < 0.001$) (Figs. 7Aa–7Af, 7B). Administration of 30-µM RSV attenuated the expression of acetyl-p53 in the RGCs to approximately control levels (1.5 ± 1.3%; $P = 0.979$) (Figs. 7Aa–7Ac, 7Aj–7Al, 7B), whereas 3-µM RSV injections did not (5.7 ± 1.6%; $P = 0.799$) (Figs. 7Ag–7Ai, 7B). In the group receiving 30-µM RSV injections alone, no significant difference was observed compared with the control group (1.1 ± 1.2%; $P > 0.999$) (Figs. 7Am–7Ao, 7B). Acetyl-p53 protein levels of whole retina in western blot analysis showed similar pattern in all groups (Supplementary Fig. S2).

Investigative Ophthalmology & Visual Science

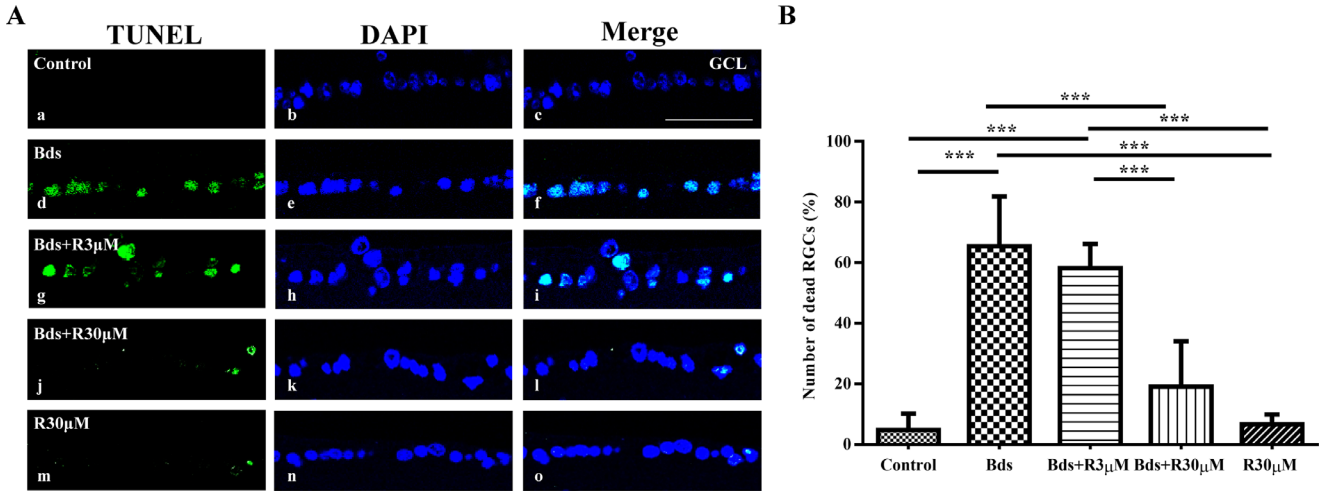

Figure 6. Quantitative analysis of RGC death among the five groups. (**A**) Representative photographs of dead RGC staining (green) by TUNEL assay of all groups at day 21 post-injection. Nuclei were labeled with DAPI staining (blue). (**B**) The percentages of TUNEL-positive RGCs in all labeled RGCs by DAPI staining in the GCL were measured. *Scale bar*: 50 µm. The data are presented as the mean ± SD ($n = 6$). Asterisks indicate statistical differences ($^{*}P < 0.05$, $^{**}P < 0.01$, $^{***}P < 0.001$) as determined by one-way ANOVA with Tukey as post hoc test. Control, PBS injection group; Bds, microbead injection group; Bds+R3µM, microbead injection with 3-µM RSV injection group; Bds+R30µM, microbead injection with 30-µM RSV injection group; R30µM, 30-µM RSV injection alone group.

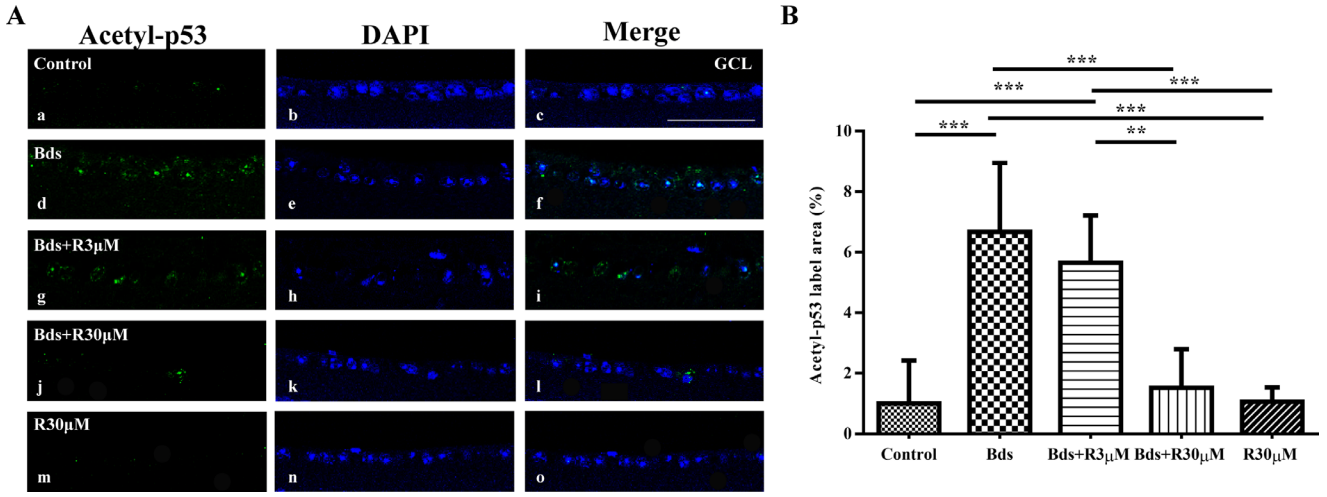

Figure 7. Quantitative analysis of acetyl-p53 expression among the five groups. (**A**) Representative photographs of acetyl-p53 (green) expression in RGCs of all groups at day 21 post-injection. Nuclei were labeled with DAPI staining (blue). (**B**) The percentages of acetyl-p53-labeled areas in the GCL were measured. *Scale bar*: 50 µm. The data are presented as the mean ± SD ($n = 6$). Asterisks indicate statistical differences ($^{*}P < 0.05$, $^{**}P < 0.01$, $^{***}P < 0.001$) as determined by one-way ANOVA with Tukey as post hoc test. Control, PBS injection group; Bds, microbead injection group; Bds+R3µM, microbead injection with 3-µM RSV injection group; Bds+R30µM, microbead injection with 30-µM RSV injection group; R30µM, 30-µM RSV injection alone group.

RSV-Induced MGC Activates and Changes BDNF Expression in Mice Under High IOP

We investigated the cellular correlation between gene expression in RGCs and MGCs in response to RSV treatment. As shown in Figures 8A and 8B, RSV upregulated the expression of GFAP in a dose-dependent manner in microbead-injected eyes. Microbead injection with either 3-µM or 30-µM RSV increased the GFAP fluorescence area (3.9 ± 0.2% vs. 13.8 ± 3.8%) compared with the control group (1.8 ± 0.4%; $P = 0.598$ vs. $P < 0.001$) (Figs. 8Aa–8Ac, 8Ag–8Al, 8B). Smaller numbers of GFAP-positive areas were noted in the microbead-injected group and the group receiving RSV injections alone compared with the control group (2.3 ± 0.2% vs. 2.5 ± 0.4%; $P = 0.995$ vs. $P = 0.98$) (Figs. 8Ad–8Af, 8Am–8Ao, 8B).

As shown in Figures 8C and 8D, mouse retinas were double-stained using anti-BDNF and anti-GS antibodies. Significantly lower BDNF expression was noted in the inner nuclear layer of microbead-injected eyes (6.0 ± 4.5%) (Figs. 8Ce–8Ch, 8D) compared to controls (12.9 ± 4.9%) (Figs. 8Ca–8Cd, 8D) ($P < 0.05$). Microbead injection with

Investigative Ophthalmology & Visual Science

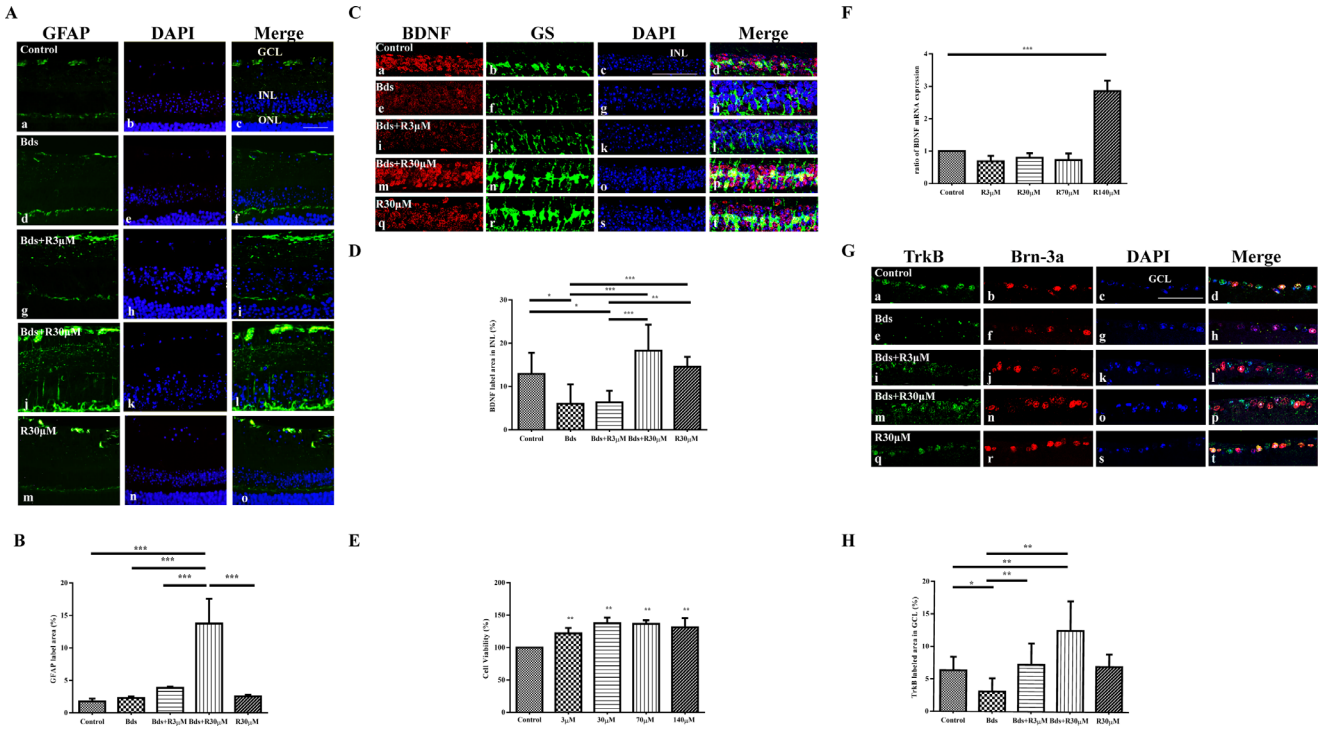

Figure 8. Quantitative analysis of GFAP, BDNF, and TrkB expression in MGCs and RGCs among the five groups and BDNF expression after administration of RSV in cultured MGCs. (**A**) Representative photographs of GFAP (green) expression in retina in all groups at day 21 post-injection. (**B**) The percentages of GFAP-labeled fluorescence area in the retina were measured. (**C**) Representative photographs of double immunofluorescence staining for BDNF (red) and GS (green) expression in the INL in all groups at day 21 post-injection. (**D**) The percentages of BDNF-labeled fluorescence area in the INL were measured. (**E**) Cell viability was assessed by CCK-8 assay. MGCs were treated with RSV for 24 hours at various concentrations. (**F**) Levels of mRNA for BDNF were standardized to β-actin mRNA levels amplified using the same RNA sample from cultured MGCs after administration of RSV at different concentrations (0.2% DMSO in DMEM as control; 3-μM, 30-μM, 70-μM, and 140-μM RSV). (**G**) Representative photographs of double immunofluorescence staining for TrkB (green) and Brn-3a (red) expression in the GCL in all groups at day 21 post-injection. (**H**) The percentages of TrkB-labeled fluorescence areas in the GCL were measured. *Scale bar*: 50 μm. The data are presented as the mean ± SD ($n = 6$). Asterisks indicate statistical differences ($^{*}P < 0.05$, $^{**}P < 0.01$, $^{***}P < 0.001$) as determined by one-way ANOVA with Tukey as post hoc test. INL, inner nuclear layer; ONL, outer nuclear layer; Control, PBS injection group; Bds, microbead injection group; Bds+R3μM, microbead injection with 3-μM RSV injection group; Bds+R30μM, microbead injection with 30-μM RSV injection group; R30μM, 30-μM RSV injection alone group.

30-μM RSV increased the expression of BDNF compared with microbead injection alone (18.3 ± 6.0%; $P < 0.001$) (Figs. 8Cm–8Cp, 8D). There was no significant increase in the expression of BDNF as a result of injections of 30-μM RSV alone compared with the control group (14.6 ± 5.6%; $P = 0.558$) (Figs. 8Cq–8Ct, 8D). BDNF protein levels of whole retina in western blot analysis showed similar patterns in all groups (Supplementary Fig. S3). To investigate that this observed change in expression could be from MGCs, we also studied the gene expression of BDNF in the cultured MGCs exposed to RSV at concentrations of 3, 30, 70, and 140 μM in vitro. We investigated the viability of cultured MGCs exposed to each concentration of RSV. Figure 8E shows that MGC viability increased in response to each of the concentrations of RSV treatment ($P < 0.01$), indicating that RSV and the vehicle are not toxic to the cultured MGCs. Gene expression of BDNF significantly increased by 2.9-fold compared to the control ($P < 0.001$) (Fig. 8F) following treatment with RSV at a concentration of 140 μM, but was not affected at concentrations of 3 μM, 30 μM, or 70 μM. Furthermore, we analyzed the expression of TrkB in RGCs (Figs. 8G, 8H). Mouse retinae were double-stained using anti-Brn-3a and anti-TrkB antibodies. TrkB-immunolabeled areas were observed in the GCL of controls (6.4 ± 2.1%) (Figs. 8Ga–8Gd, 8H). TrkB expression was markedly diminished in the microbead injection group compared with the control group (3.1 ± 2.0%; $P < 0.05$) (Figs. 8Ge–8Gh, 8H). Microbead injection with either 3-μM or 30-μM RSV significantly upregulated the expression of TrkB compared with microbead injection alone (7.3 ± 3.3% and 12.5 ± 4.6%, respectively; $P < 0.01$) (Figs. 8Gi–8Gp, 8H). Administration of 30-μM RSV alone did not significantly alter the expression of TrkB compared with controls (7.0 ± 4.7%; $P = 0.999$) (Figs. 8Gq–8Gt, 8H). In western blot analysis, TrkB protein levels of whole retina showed similar patterns in all groups (Supplementary Fig. S4).

Discussion

It has been proposed that elevated IOP may accelerate oxidative adduct formation in retinal cells and block axonal protein transport of RGCs, leading to neurotrophic factor deficiency and apoptotic RGCs death.[71] Previous studies involving mouse models of glaucoma suggest that an increase in oxidative stress is an early event in RGCs

exposed to elevated IOP.[72] The present study showed that intravitreal administration of 30-μM RSV markedly increased Sirt1 expression and decreased the generation of ROS in RGCs, ameliorated the expression of Brn-3a and SMI-32, and resulted in a drastic decrease in TUNEL-positive cells in RGCs. RSV is a well-known antioxidant that acts by suppressing ROS generation via the induction of superoxide dismutase, catalase, and glutathione peroxidase 1.[73] Luna et al.[74] reported that RSV treatment inhibited intracellular ROS generation in cultured trabecular meshwork cells after chronic oxidative injury.

Activated Sirt1 deacetylates p53 and therefore plays a critical role in stress responses in various types of cells.[75–77] He et al.[78] demonstrated that activation of Sirt1 inhibited H_2O_2-induced apoptosis in mouse osteoblast cells by decreasing p53 acetylation. Liu et al.[23] reported an interesting association between ROS and p53, where ROS triggered p53 activation and p53 in turn regulated cellular ROS generation. In the present study, we showed that intravitreal administration of RSV markedly decreased the expression of acetylated p53 and ROS generation in RGCs. Taken together, these results support the theory that Sirt1 activation by RSV leads to p53 deacetylation in RGCs and regulation of ROS generation, which may protect rescue RGCs from high IOP-induced cell death.

MGCs produce neurotrophic factors that directly or indirectly affect the survival of neurons in the retina.[38] It has been reported that MGC activation may be relevant to the development and cure of various ocular diseases, including diabetic retinopathy, retinal trauma, choroidal neovascularization, retinal detachment, and age-related macular degeneration (AMD).[38,40,79–82] Our previous study also revealed that intravitreal administration of RSV in a murine AMD model induces activation of MGCs and promotes regression of choroidal neovascularization, demonstrating its potential as a novel therapeutic approach.[40] Interestingly, activated MGCs have also been detected in human donor eyes with glaucoma[83,84]; however, the correlation between development of glaucoma and activation of MGCs is not fully understood.

Gambert et al.[85] showed that MGC activation enhances their capacity to provide metabolic support for RGCs and therefore has a potential role in protecting RGCs during the development of glaucoma. Harada et al.[42] reported that activated MGCs change the gene profile and expression of a variety of molecules, including BDNF, which is upregulated up to 4.4-fold compared with controls in cultured MGCs that have been exposed to 1-μM brimonidine. They also concluded that the expression of BDNF by MGCs was important for the survival of RGCs. We demonstrated that BDNF gene expression was upregulated up to 2.9-fold compared with controls following exposure to 140-μM RSV. Furthermore, the upregulation of TrkB expression in RGCs was confirmed in this study.

These results show that RSV enhances BDNF–TrkB signaling between MGCs and RGCs, a process that is important for protecting RGCs from cell death. In addition, we revealed that RSV-induced MGC activation was detected in eyes with high IOP but not in those with normal IOP and RSV alone. In human eyes with AMD, MGC activation has been detected around the choroidal–neovascularization lesion but not in the area of the healthy retina.[86] Although the mechanism behind the specific activation of MGCs by RSV is still unclear, this unique phenomenon suggests that intravitreal administration of RSV may alleviate retinal lesions.

Previous studies have reported that oral or intraperitoneal administration of RSV may prevent RGC death by blocking the Bax-caspase3-dependent apoptotic pathway[87] and the activity of NF-κB[34] in RGCs of an animal model for glaucoma with ischemia-reperfusion injury; however, the underlying mechanism is not fully understood. Furthermore, it is interesting to note that Luna et al.[74] showed that RSV treatment prevented increased production of intracellular ROS and inflammatory markers such as IL-1, IL-6, and IL-8 due to chronic oxidative stress in cultured trabecular meshwork cells, suggesting that RSV could potentially may have a role in preventing several types of cells abnormalities observed in glaucoma.

We demonstrated that intravitreal administration of RSV markedly decreases ROS generation and acetylated p53 expression in RGCs, which rescues them from high IOP-induced cell death. Furthermore, we found that ocular administration of RSV also activates MGCs, resulting in upregulation of BDNF and TrkB expression in RGCs, which in turn increases RGC survival. These results are consistent with previous studies and showcase new evidence that highlights the therapeutic potential of RSV in glaucoma. Moreover, it has been reported that the half-life of RSV by oral administration is 8 to 14 minutes in a human body.[88] In the present study, we used a single intravitreal injection of RSV and observed the neuroprotective effect 21 days from the date of administration; our results indicate that RSV has a long-lasting effect in the intraocular environment. Shindler et al.[89] also showed that a single intravitreal administration of SRT501, a formulation of RSV, provided strong neuroprotection for 30 days. It is known that eyes form the blood–retina barrier to control the exchange of nutrients, as in the brain. Sawda et al.[90] demonstrated that RSV crosses the blood–brain barrier, but very low concentrations are found in the brain. This may mean that the blood–retina barrier blocks RSV clearance from the eyes and concentrates RSV on the inside of the eyes; thus, intravitreal administration allows for a long-term effect of RSV.

A limitation of our study was that the immunohistochemistry of GFAP was used to detect activated MGCs, despite the fact that there are other activated glial cells in the retina that also express GFAP, such as astrocytes and microglia; however, MGCs account for approximately 90% of the population of the glial cells in the retina. In addition, the MGCs span across the entire retina and their morphology differs from that of astrocytes and microglia. In the present study, we observed many GFAP-positive cells that spanned across the entire retina, a distribution pattern indicating that they were indeed activated MGCs. Rather than confirming the activation of MGCs by RSV in vivo, we examined this cause-and-effect relationship using cultured MGCs in vitro. Another limitation was that the effect of RSV on retinal function has not been fully studied. To our knowledge, our results are the first to show a link between RGCs and MGCs by RSV treatment, although it has been known that many types of cells cooperate and interact to maintain retinal homeostasis. The present study adds to our understanding of the interaction between RGCs and MGCs by revealing the novel mechanism of RGCs protection by RSV. Further studies are needed to understand the relationship between RSV and retinal function. In summary, the present study demonstrated that intravitreal administration of RSV significantly

Investigative Ophthalmology & Visual Science

rescues RGCs from high IOP-induced cell death via multiple pathways and may therefore have therapeutic potential against glaucoma.

Acknowledgments

The authors thank Ken-ichi Nakahama, PhD (Department of Cellular Physiological Chemistry, Tokyo Medical and Dental University), for his technical support.

Supported by a Bayer Retina Award grant.

Disclosure: **K. Cao**, None; **T. Ishida**, None; **Y. Fang**, None; **K. Shinohara**, None; **X. Li**, None; **N. Nagaoka**, None; **K. Ohno-Matsui**, None; **T. Yoshida**, None

References

1. Quigley HA, Broman AT. The number of people with glaucoma worldwide in 2010 and 2020. *Br J Ophthalmol*. 2006;90:262–267.
2. Dandona L, Dandona R. What is the global burden of visual impairment? *BMC Med*. 2006;4:6.
3. Jiang SM, Zeng LP, Zeng JH, Tang L, Chen XM, Wei X. β-III-Tubulin: a reliable marker for retinal ganglion cell labeling in experimental models of glaucoma. *Int J Ophthalmol*. 2015;8:643–652.
4. Crish SD, Calkins DJ. Neurodegeneration in glaucoma: progression and calcium-dependent intracellular mechanisms. *Neuroscience*. 2011;176:1–11.
5. Gordon MO, Beiser JA, Brandt JD, et al. The Ocular Hypertension Treatment Study: baseline factors that predict the onset of primary open-angle glaucoma. *Arch Ophthalmol*. 2002;120:714–720; discussion 829–730.
6. Coleman MP, Perry VH. Axon pathology in neurological disease: a neglected therapeutic target. *Trends Neurosci*. 2002;25:532–537.
7. Heijl A, Leske MC, Bengtsson B, Hyman L, Bengtsson B, Hussein M. Reduction of intraocular pressure and glaucoma progression: results from the Early Manifest Glaucoma Trial. *Arch Ophthalmol*. 2002;120:1268–1279.
8. McKinnon SJ, Goldberg LD, Peeples P, Walt JG, Bramley TJ. Current management of glaucoma and the need for complete therapy. *Am J Manag Care*. 2008;14(suppl 1):S20–S27.
9. Danesh-Meyer HV. Neuroprotection in glaucoma: recent and future directions. *Curr Opin Ophthalmol*. 2011;22:78–86.
10. Betteridge DJ. What is oxidative stress? *Metabolism*. 2000;49:3–8.
11. Emerit J, Edeas M, Bricaire F. Neurodegenerative diseases and oxidative stress. *Biomed Pharmacother*. 2004;58:39–46.
12. Hsieh HL, Yang CM. Role of redox signaling in neuroinflammation and neurodegenerative diseases. *BioMed Res Int*. 2013;2013:484613.
13. Yamamoto K, Maruyama K, Himori N, et al. The novel Rho kinase (ROCK) inhibitor K-115: a new candidate drug for neuroprotective treatment in glaucoma. *Invest Ophthalmol Vis Sci*. 2014;55:7126–7136.
14. Wan P, Su W, Zhang Y, Li Z, Deng C, Zhuo Y. Trimetazidine protects retinal ganglion cells from acute glaucoma via the Nrf2/Ho-1 pathway. *Clin Sci (Lond)*. 2017;131:2363–2375.
15. Qi Y, Chen L, Zhang L, Liu WB, Chen XY, Yang XG. Crocin prevents retinal ischaemia/reperfusion injury-induced apoptosis in retinal ganglion cells through the PI3K/AKT signalling pathway. *Exp Eye Res*. 2013;107:44–51.
16. Smedowski A, Liu X, Podracka L, et al. Increased intraocular pressure alters the cellular distribution of HuR protein in retinal ganglion cells - a possible sign of endogenous neuroprotection failure. *Biochim Biophys Acta*. 2018;1864:296–306.
17. Guo Y, Johnson E, Cepurna W, Jia L, Dyck J, Morrison JC. Does elevated intraocular pressure reduce retinal TRKB-mediated survival signaling in experimental glaucoma? *Exp Eye Res*. 2009;89:921–933.
18. Wilson AM, Morquette B, Abdouh M, et al. ASPP1/2 regulate p53-dependent death of retinal ganglion cells through PUMA and Fas/CD95 activation in vivo. *J Neurosci*. 2013;33:2205–2216.
19. Wilson AM, Chiodo VA, Boye SL, Brecha NC, Hauswirth WW, Di Polo A. Inhibitor of apoptosis-stimulating protein of p53 (iASPP) is required for neuronal survival after axonal injury. *PLoS One*. 2014;9:e94175.
20. Lin HJ, Chen WC, Tsai FJ, Tsai SW. Distributions of p53 codon 72 polymorphism in primary open angle glaucoma. *Br J Ophthalmol*. 2002;86:767–770.
21. Ressiniotis T, Griffiths PG, Birch M, Keers S, Chinnery PF. Primary open angle glaucoma is associated with a specific p53 gene haplotype. *J Med Genet*. 2004;41:296–298.
22. Daugherty CL, Curtis H, Realini T, Charlton JF, Zareparsi S. Primary open angle glaucoma in a Caucasian population is associated with the p53 codon 72 polymorphism. *Mol Vis*. 2009;15:1939–1944.
23. Liu B, Chen Y, St Clair DK. ROS and p53: a versatile partnership. *Free Radic Biol Med*. 2008;44:1529–1535.
24. Zhang Y, Zhang Y, Zhong C, Xiao F. Cr(VI) induces premature senescence through ROS-mediated p53 pathway in L-02 hepatocytes. *Sci Rep*. 2016;6:34578.
25. Yuan Y, Cruzat VF, Newsholme P, Cheng J, Chen Y, Lu Y. Regulation of SIRT1 in aging: roles in mitochondrial function and biogenesis. *Mech Ageing Dev*. 2016;155:10–21.
26. Kulkarni SS, Canto C. The molecular targets of resveratrol. *Biochim Biophys Acta*. 2015;1852:1114–1123.
27. Elmadhun NY, Sabe AA, Robich MP, Chu LM, Lassaletta AD, Sellke FW. The pig as a valuable model for testing the effect of resveratrol to prevent cardiovascular disease. *Ann N Y Acad Sci*. 2013;1290:130–135.
28. Jang M, Cai L, Udeani GO, et al. Cancer chemopreventive activity of resveratrol, a natural product derived from grapes. *Science*. 1997;275:218–220.
29. Lancon A, Michaille JJ, Latruffe N. Effects of dietary phytophenols on the expression of microRNAs involved in mammalian cell homeostasis. *J Sci Food Agric*. 2013;93:3155–3164.
30. Tome-Carneiro J, Larrosa M, Gonzalez-Sarrias A, Tomas-Barberan FA, Garcia-Conesa MT, Espin JC. Resveratrol and clinical trials: the crossroad from in vitro studies to human evidence. *Curr Pharm Des*. 2013;19:6064–6093.
31. Gupta C, Prakash D. Phytonutrients as therapeutic agents. *J Complement Integr Med*. 2014;11:151–169.
32. Aguirre L, Fernandez-Quintela A, Arias N, Portillo MP. Resveratrol: anti-obesity mechanisms of action. *Molecules*. 2014;19:18632–18655.
33. Ray PS, Maulik G, Cordis GA, Bertelli AA, Bertelli A, Das DK. The red wine antioxidant resveratrol protects isolated rat hearts from ischemia reperfusion injury. *Free Rad Biol Med*. 1999;27:160–169.
34. Dong W, Li F, Pan Z, et al. Resveratrol ameliorates subacute intestinal ischemia-reperfusion injury. *J Surg Res*. 2013;185:182–189.
35. Yulug E, Turedi S, Karaguzel E, Kutlu O, Mentese A, Alver A. The short term effects of resveratrol on ischemia-reperfusion injury in rat testis. *J Pediatr Surg*. 2014;49:484–489.

36. Yu HP, Hwang TL, Hsieh PW, Lau YT. Role of estrogen receptor-dependent upregulation of P38 MAPK/heme oxygenase 1 in resveratrol-mediated attenuation of intestinal injury after trauma-hemorrhage. *Shock*. 2011;35:517–523.
37. Pirhan D, Yuksel N, Emre E, Cengiz A, Kursat Yildiz D. Riluzole- and resveratrol-induced delay of retinal ganglion cell death in an experimental model of glaucoma. *Curr Eye Res*. 2016;41:59–69.
38. Reichenbach A, Bringmann A. New functions of Müller cells. *Glia*. 2013;61:651–678.
39. Jablonski MM, Tombran-Tink J, Mrazek DA, Iannaccone A. Pigment epithelium-derived factor supports normal Müller cell development and glutamine synthetase expression after removal of the retinal pigment epithelium. *Glia*. 2001;35:14–25.
40. Ishida T, Yoshida T, Shinohara K, et al. Potential role of Sirtuin 1 in Müller glial cells in mice choroidal neovascularization. *PLoS One*. 2017;12:e0183775.
41. Abrahan CE, Insua MF, Politi LE, German OL, Rotstein NP. Oxidative stress promotes proliferation and dedifferentiation of retina glial cells in vitro. *J Neurosci Res*. 2009;87:964–977.
42. Harada C, Guo X, Namekata K, et al. Glia- and neuron-specific functions of TrkB signalling during retinal degeneration and regeneration. *Nat Commun*. 2011;2:189.
43. Harada T, Harada C, Nakamura K, et al. The potential role of glutamate transporters in the pathogenesis of normal tension glaucoma. *J Clin Invest*. 2007;117:1763–1770.
44. Bunker S, Holeniewska J, Vijay S, et al. Experimental glaucoma induced by ocular injection of magnetic microspheres. *J Vis Exp*. 2015;96:52400.
45. Matsumoto Y, Kanamori A, Nakamura M, Negi A. Rat chronic glaucoma model induced by intracameral injection of microbeads suspended in sodium sulfate-sodium hyaluronate. *Jpn J Ophthalmol*. 2014;58:290–297.
46. Kitamura Y, Bikbova G, Baba T, Yamamoto S, Oshitari T. In vivo effects of single or combined topical neuroprotective and regenerative agents on degeneration of retinal ganglion cells in rat optic nerve crush model. *Sci Rep*. 2019;9:101.
47. Tual-Chalot S, Allinson KR, Fruttiger M, Arthur HM. Whole mount immunofluorescent staining of the neonatal mouse retina to investigate angiogenesis in vivo. *J Vis Exp*. 2013;77:e50546.
48. Murata H, Aihara M, Chen YN, Ota T, Numaga J, Araie M. Imaging mouse retinal ganglion cells and their loss in vivo by a fundus camera in the normal and ischemia-reperfusion model. *Invest Ophthalmol Vis Sci*. 2008;49:5546–5552.
49. Domenici L, Origlia N, Falsini B, et al. Rescue of retinal function by BDNF in a mouse model of glaucoma. *PLoS One*. 2014;9:e115579.
50. Ruzafa N, Pereiro X, Aspichueta P, Araiz J, Vecino E. The retina of osteopontin deficient mice in aging. *Mol Neurobiol*. 2018;55:213–221.
51. Zhang H, Li X, Dai X, et al. The degeneration and apoptosis patterns of cone photoreceptors in rd11 mice. *J Ophthalmol*. 2017;2017:9721362.
52. Kumar V, Mesentier-Louro LA, Oh AJ, et al. Increased ER stress after experimental ischemic optic neuropathy and improved RGC and oligodendrocyte survival after treatment with chemical chaperon. *Invest Ophthalmol Vis Sci*. 2019;60:1953–1966.
53. Zhang L, Li G, Shi M, et al. Establishment and characterization of an acute model of ocular hypertension by laser-induced occlusion of episcleral veins. *Invest Ophthalmol Vis Sci*. 2017;58:3879–3886.
54. Jia Y, Jiang S, Chen C, et al. Caffeic acid phenethyl ester attenuates nuclear factor-κB-mediated inflammatory responses in Müller cells and protects against retinal ganglion cell death. *Mol Med Rep*. 2019;19:4863–4871.
55. Grishagin IV. Automatic cell counting with ImageJ. *Anal Biochem*. 2015;473:63–65.
56. Yang Q, Cho KS, Chen H, et al. Microbead-induced ocular hypertensive mouse model for screening and testing of aqueous production suppressants for glaucoma. *Invest Ophthalmol Vis Sci*. 2012;53:3733–3741.
57. Sappington RM, Carlson BJ, Crish SD, Calkins DJ. The microbead occlusion model: a paradigm for induced ocular hypertension in rats and mice. *Invest Ophthalmol Vis Sci*. 2010;51:207–216.
58. Trost A, Motloch K, Bruckner D, et al. Time-dependent retinal ganglion cell loss, microglial activation and blood-retina-barrier tightness in an acute model of ocular hypertension. *Exp Eye Res*. 2015;136:59–71.
59. McGrady NR, Minton AZ, Stankowska DL, He S, Jefferies HB, Krishnamoorthy RR. Upregulation of the endothelin A (ETA) receptor and its association with neurodegeneration in a rodent model of glaucoma. *BMC Neurosci*. 2017;18:27.
60. Yang Y, Mao D, Chen X, et al. Decrease in retinal neuronal cells in streptozotocin-induced diabetic mice. *Mol Vis*. 2012;18:1411–1420.
61. Mead B, Thompson A, Scheven BA, Logan A, Berry M, Leadbeater W. Comparative evaluation of methods for estimating retinal ganglion cell loss in retinal sections and whole-mounts. *PLoS One*. 2014;9:e110612.
62. Johnson-Cadwell LI, Jekabsons MB, Wang A, Polster BM, Nicholls DG. 'Mild uncoupling' does not decrease mitochondrial superoxide levels in cultured cerebellar granule neurons but decreases spare respiratory capacity and increases toxicity to glutamate and oxidative stress. *J Neurochem*. 2007;101:1619–1631.
63. Boriushkin E, Wang JJ, Li J, Jing G, Seigel GM, Zhang SX. Identification of p58IPK as a novel neuroprotective factor for retinal neurons. *Invest Ophthalmol Vis Sci*. 2015;56:1374–1386.
64. Ou K, Mertsch S, Theodoropoulou S, et al. Restoring retinal neurovascular health via substance P. *Exp Cell Res*. 2019;380:115–123.
65. Jensen EC. Quantitative analysis of histological staining and fluorescence using ImageJ. *Anat Rec (Hoboken)*. 2013;296:378–381.
66. Feng M, Zhong L-X, Zhan Z-Y, Huang Z-H, Xiong J-P. Resveratrol treatment inhibits proliferation of and induces apoptosis in human colon cancer cells. *Med Sci Monit*. 2016;22:1101–1108.
67. Gu R, Ding X, Tang W, Lei B, Jiang C, Xu G. A synthesized glucocorticoid-induced leucine zipper peptide inhibits retinal Müller cell gliosis. *Front Pharmacol*. 2018;9:331–331.
68. Bao Y, Liu F, Liu X, et al. Methyl 3,4-dihydroxybenzoate protects retina in a mouse model of acute ocular hypertension through multiple pathways. *Exp Eye Res*. 2019;181:15–24.
69. Gao S, Andreeva K, Cooper NG. Ischemia-reperfusion injury of the retina is linked to necroptosis via the ERK1/2-RIP3 pathway. *Mol Vis*. 2014;20:1374–1387.
70. Nadal-Nicolas FM, Jimenez-Lopez M, Sobrado-Calvo P, et al. Brn3a as a marker of retinal ganglion cells: qualitative and quantitative time course studies in naive and optic nerve-injured retinas. *Invest Ophthalmol Vis Sci*. 2009;50:3860–3868.
71. Weinreb RN, Khaw PT. Primary open-angle glaucoma. *Lancet*. 2004;363:1711–1720.
72. Liu Q, Ju WK, Crowston JG, et al. Oxidative stress is an early event in hydrostatic pressure induced retinal ganglion cell damage. *Invest Ophthalmol Vis Sci*. 2007;48:4580–4589.

Investigative Ophthalmology & Visual Science

73. Xia N, Daiber A, Habermeier A, et al. Resveratrol reverses endothelial nitric-oxide synthase uncoupling in apolipoprotein E knockout mice. *J Pharmacol Exp Ther*. 2010;335:149–154.
74. Luna C, Li G, Liton PB, et al. Resveratrol prevents the expression of glaucoma markers induced by chronic oxidative stress in trabecular meshwork cells. *Food Chem Toxicol*. 2009;47:198–204.
75. Rahman S, Islam R. Mammalian Sirt1: insights on its biological functions. *Cell Commun Signal*. 2011;9:11.
76. Kim EJ, Kho JH, Kang MR, Um SJ. Active regulator of SIRT1 cooperates with SIRT1 and facilitates suppression of p53 activity. *Mol Cell*. 2007;28:277–290.
77. Vaziri H, Dessain SK, Ng Eaton E, et al. hSIR2(SIRT1) functions as an NAD-dependent p53 deacetylase. *Cell*. 2001;107:149–159.
78. He N, Zhu X, He W, Zhao S, Zhao W, Zhu C. Resveratrol inhibits the hydrogen dioxide-induced apoptosis via Sirt 1 activation in osteoblast cells. *Biosci Biotechnol Biochem*. 2015;79:1779–1786.
79. Lu YB, Iandiev I, Hollborn M, et al. Reactive glial cells: increased stiffness correlates with increased intermediate filament expression. *FASEB J*. 2011;25:624–631.
80. Berk BA, Vogler S, Pannicke T, et al. Brain-derived neurotrophic factor inhibits osmotic swelling of rat retinal glial (Müller) and bipolar cells by activation of basic fibroblast growth factor signaling. *Neuroscience*. 2015;295:175–186.
81. Bringmann A, Iandiev I, Pannicke T, et al. Cellular signaling and factors involved in Müller cell gliosis: neuroprotective and detrimental effects. *Prog Retin Eye Res*. 2009;28:423–451.
82. Garcia M, Forster V, Hicks D, Vecino E. Effects of Müller glia on cell survival and neuritogenesis in adult porcine retina in vitro. *Invest Ophthalmol Vis Sci*. 2002;43:3735–3743.
83. Wang L, Cioffi GA, Cull G, Dong J, Fortune B. Immunohistologic evidence for retinal glial cell changes in human glaucoma. *Invest Ophthalmol Vis Sci*. 2002;43:1088–1094.
84. Gallego BI, Salazar JJ, de Hoz R, et al. IOP induces upregulation of GFAP and MHC-II and microglia reactivity in mice retina contralateral to experimental glaucoma. *J Neuroinflammation*. 2012;9:92.
85. Gambert S, Gabrielle PH, Masson E, et al. Cholesterol metabolism and glaucoma: modulation of Müller cell membrane organization by 24S-hydroxycholesterol. *Chem Phys Lipids*. 2017;207:179–191.
86. Madigan MC, Penfold PL, Provis JM, Balind TK, Billson FA. Intermediate filament expression in human retinal macroglia. Histopathologic changes associated with age-related macular degeneration. *Retina*. 1994;14:65–74.
87. Luo H, Zhuang J, Hu P, et al. Resveratrol delays retinal ganglion cell loss and attenuates gliosis-related inflammation from ischemia-reperfusion injury. *Invest Ophthalmol Vis Sci*. 2018;59:3879–3888.
88. Walle T, Hsieh F, DeLegge MH, Oatis JE, Jr, Walle UK. High absorption but very low bioavailability of oral resveratrol in humans. *Drug Metab Dispos*. 2004;32:1377–1382.
89. Shindler KS, Ventura E, Rex TS, Elliott P, Rostami A. SIRT1 activation confers neuroprotection in experimental optic neuritis. *Invest Ophthalmol Vis Sci*. 2007;48:3602–3609.
90. Sawda C, Moussa C, Turner RS. Resveratrol for Alzheimer's disease. *Ann N Y Acad Sci*. 2017;1403:142–149.

Investigative Ophthalmology & Visual Science